

## Height distribution between cloud and aerosol layers from the GLAS spaceborne lidar in the Indian Ocean region

William D. Hart,<sup>1</sup> James D. Spinhirne,<sup>2</sup> Steven P. Palm,<sup>1</sup> and Dennis L. Hlavka<sup>1</sup>

Received 31 May 2005; revised 26 July 2005; accepted 24 August 2005; published 30 September 2005.

[1] The Geoscience Laser Altimeter System (GLAS), a nadir pointing lidar on the Ice Cloud and land Elevation Satellite (ICESat) launched in 2003, now provides important new global measurements of the relationship between the height distribution of cloud and aerosol layers. GLAS data have the capability to detect, locate, and distinguish between cloud and aerosol layers in the atmosphere up to 40 km altitude. The data product algorithm tests the product of the maximum attenuated backscatter coefficient  $b'(r)$  and the vertical gradient of  $b'(r)$  within a layer against a predetermined threshold. An initial case result for the critical Indian Ocean region is presented. From the results the relative height distribution between collocated aerosol and cloud shows extensive regions where cloud formation is well within dense aerosol scattering layers at the surface. **Citation:** Hart, W. D., J. D. Spinhirne, S. P. Palm, and D. L. Hlavka (2005), Height distribution between cloud and aerosol layers from the GLAS spaceborne lidar in the Indian Ocean region, *Geophys. Res. Lett.*, 32, L22S06, doi:10.1029/2005GL023671.

### 1. Introduction

[2] Both cloud and aerosols have important direct effects on the radiation balance of the earth. They influence the incoming solar energy by changing the albedo of the earth-atmosphere system and if absorbing they provide an increase in atmospheric radiative heating rates through the vertical range of their distribution. In addition, cloud and aerosol particles can interact with each other to produce significant secondary influences. For instance, *Twomey* [1974] describes how certain types of aerosols can increase low-cloud droplet concentrations, which would reduce incoming energy by increasing albedo without reducing the compensatory thermally emitted energy as much, and hence would be a cooling influence. More recent modeling studies [*Ackerman et al.*, 2003] support this theory while some satellite observations [*Platnick et al.*, 2000] seem to counter it. Opposed to the enhancement of low cloud cover by aerosol layers, there is evidence [*Ackerman et al.*, 2000] that heating by aerosol particles such as soot can reduce low cloud cover by absorbing incoming solar radiation. This is done both by evaporating cloud particles and stabilizing the boundary layer by preferred heating of its top. The interaction between aerosol and clouds are now also thought to be a major influence on precipitation [*Rosenfeld*, 2000].

<sup>1</sup>Science Systems and Applications, Inc., NASA Goddard Space Flight Center, Code 613.1, Greenbelt, Maryland, USA.

<sup>2</sup>NASA Goddard Space Flight Center, Code 613.1, Greenbelt, Maryland, USA.

[3] These examples of the opposing influences that the presence of aerosol has on the distribution and characteristics of cloud cover serve to illustrate the complexity of the atmospheric cloud-aerosol system. In order to quantify the effects that they impose on the earth's radiation balance, it is necessary that the global distribution of clouds and aerosol layers, especially with regard to their coincident occurrences, be well known. The height distribution of aerosol radiative forcing needs to be known separately and with correct clearing of cloud scattering [*Coakley et al.*, 2002]. In addition, the height distribution is an issue for the remote sensing of clouds. If there is significant aerosol scattering and absorption above cloud or elevated within clouds, passive multi-spectral techniques may be in error [*Sekiguchi et al.*, 2003]. Satellite observations provide a potential opportunity to find these distributions globally if the signals from the aerosols and clouds can be separated and vertically located. Spaceborne lidar offers a means to derive these kinds of products from backscatter measurements.

[4] The Geoscience Laser Altimeter System (GLAS) is a laser remote sensing instrument launched into orbit aboard ICESat in January, 2003. GLAS is a dual-purpose laser instrument, serving as both a precision surface elevation altimeter and atmospheric lidar [*Spinhirne et al.*, 2005]. Since February of 2003, GLAS has operated during discrete periods of approximately 33 days duration. When operating, it provides continuous and nearly pole-to-pole atmospheric lidar observations of clouds and aerosols through altitudes of 0–40 km. A complete description of cloud and aerosol observations and analysis resolutions is given by *Palm et al.* [2002]. GLAS is sensitive to very optically rarefied particulate layers, down to backscatter cross section below  $10^{-7}$  (m-sr)<sup>-1</sup> and is capable of detecting multiple layers to the limit of signal (optical depth < about 4.0).

[5] In this study, we introduce and present a brief summary of the GLAS cloud/aerosol algorithm. We show and discuss its strengths and weaknesses. Building on that, we present a case study in the heavily polluted Indian Ocean Region for the distribution of aerosol and clouds. We show GLAS's unique capability as a tool to accurately and comprehensively detect cloud and aerosols in the atmosphere and define their relative distribution.

### 2. Cloud/Aerosol Discrimination Technique

[6] A lidar signal is proportional to the attenuated backscatter coefficient,  $b'(r)$ . This is light backscattered from an atmospheric volume a distance  $r$  from the lidar multiplied by the intervening two way transmission. The GLAS cloud/aerosol detection and discrimination is based upon historically observed differences between cloud and aerosol layers in the magnitude of  $b'(r)$ , and the magnitude

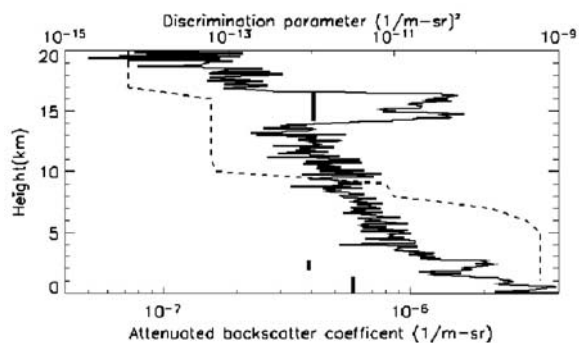


**Figure 1.** Cloud/aerosol discrimination. The solid line shows  $b'(r)$ , dashed line shows the discriminator threshold, and the vertical bars show the computed discriminator parameter for each layer. The top layer is deemed cloud, the bottom two are aerosols.

of the vertical gradient of  $b'(r)$ . At a given altitude,  $b'(r)$  and  $|d[b'(r)]/dr|$  tend to be greater in cloud layers than in aerosol layers. Because the formation and dissipation of cloud particles involves the change of phase of water between the gaseous state and liquid or solid state, while aerosol particle formation is less active, the particle size, number concentration and magnitude of inhomogeneity of cloud layers are generally greater than aerosol layers. A more complete description of the basis of GLAS cloud/aerosol discrimination is given by Palm *et al.* [2002]. A short summary follows.

[7] For each particulate layer that is detected by GLAS, values  $b'_x(r)$  and  $|d[b'(r)]/dr|_x$ , where the  $x$  indicates the maximum value in the layer, are found. The product of these is computed,  $P_l = b'_x(r) \times |d[b'(r)]/dr|_x$ , where subscript  $l$  denotes a particular layer. The parameter  $P_l$  is tested against a threshold  $T_l$ . If  $P_l$  is greater than  $T_l$ , then the layer is deemed to be a cloud. Otherwise, it is considered to be an aerosol. If higher layers are present, a transmission loss correction is applied to  $b'_x(r)$  and  $|d[b'(r)]/dr|_x$  before the product is computed. The transmission loss caused by an intervening layer is estimated using an assumed lidar ratio to compute extinction as a function of altitude and integrating the extinction to obtain optical depth and transmission.

[8] The success of the technique is wholly dependent upon using the proper values of  $T_l$ . The values used in GLAS data production were determined from analysis of atmospheric lidar data derived from the high altitude lidar, NASA ER-2 Cloud Lidar System [Spinhirne *et al.*, 1982, 1996]. In the studies, layers were manually identified as cloud or aerosols. The discrimination parameter  $P_l$  was computed for these layers. From these studies, a value of the threshold  $T_l$  was selected which would maximize the probability of selecting the correct layer species when applied in the GLAS algorithm. It was found that the optimal values of  $T_l$  are a function of altitude and so a vertical profile of  $T_l$  was developed for use in the operational GLAS algorithm. A latitudinal adjustment to  $T_l$  is also necessary since its appropriate magnitude decreases toward the polar regions. Figure 1 provides an illustration of application of the GLAS discrimination technique. Seen in the figure is the strong dependence of the discrimination

threshold with altitude. Three particulate layers are readily apparent in the profile of  $b'(r)$ . It is important to note that the lower layers are determined to be aerosol layers.

### 3. Low Level Clouds and Aerosols, October 10, 2003, Indian Ocean

[9] Cloud/aerosol discrimination is a routine product of GLAS operational processing. This coupled with the global nature of GLAS observations allows the worldwide distribution of clouds and aerosols to be observed and analyzed. The forward motion and altitude resolving capability of spaceborne lidar enable a detailed view of the relative horizontal and vertical location of clouds and aerosols. These traits allow certain types of analysis that are not possible otherwise.

[10] We focus here on a case based upon GLAS observations from the Indian Ocean from October 10, 2003, during ICESat's Laser 2a operation period, ICESat track 1189. The case was selected from this time period because the quality of GLAS data was at its peak, since the transmitted energy was highest. Continental and maritime aerosols are persistently coincident in the western Indian Ocean region. The region is generally free of high clouds.

[11] A vertical cross-section of attenuated backscatter coefficient,  $b'(r)$ , from product GLA07 [Spinhirne *et al.*, 2005], in the lowest 6-km. for the time segment 16:13:20 to 16:18:32 UTC is shown in Figure 2. The GLAS data used is at 1 Hz resulting in a 7.0 km horizontal resolution. The vertical resolution is 0.076 km. The map shows the ICESat ground track of the selected October 10 segment. Potential temperature ( $q$ , solid line) and relative humidity (RH, dashed line) from a sounding at 00 UTC, October 11, 17.03N, 54.08E are overplotted on the image. The satellite was traveling from south to north during this period. The right side of the image is closest to land. At least three segments with distinct scattering characteristics are present, denoted by A, B, and C, respectively. Maritime aerosols form the broad band of enhanced backscatter coefficient that extends nearly across the image with a top at about 2.3 km. This top coincides closely with the top of a mixed layer indicated by the  $q$  and RH profiles. The top becomes less well defined between 16:16:40 and 16:17:50 UTC, segment C. The magnitude of the  $b'(r)$  for maritime aerosols is between  $2 \times 10^{-6}$  and  $4 \times 10^{-6}$  (m-sr) $^{-1}$ . Other aerosol types, possibly continental aerosols, are seen clearly in a vertical region 2.3 to 3.1 km between 16:13:20 and 16:18:32, segment A. They have an attenuated backscatter coefficient generally below  $2 \times 10^{-6}$  (m-sr) $^{-1}$ . The small white features embedded in the aerosol layer are clouds. The magnitude of  $b'(r)$  for clouds is generally greater than  $1 \times 10^{-5}$  (m-sr) $^{-1}$  which exceeds the maximum of the color scale. A cloud element with stronger backscatter is found at 16:16:40 UTC at the top of the aerosol layer. The effects of rendering the image using 1-second average profiles cause some of the cloud elements to appear broader horizontally than they actually are. Finally, the prominent white line at 0 km is the lidar return off the ocean surface.

[12] The GLAS lidar image offers unique information on the relationship between the aerosols and the clouds. The magnitude of the of the aerosol lidar signal is presumed to

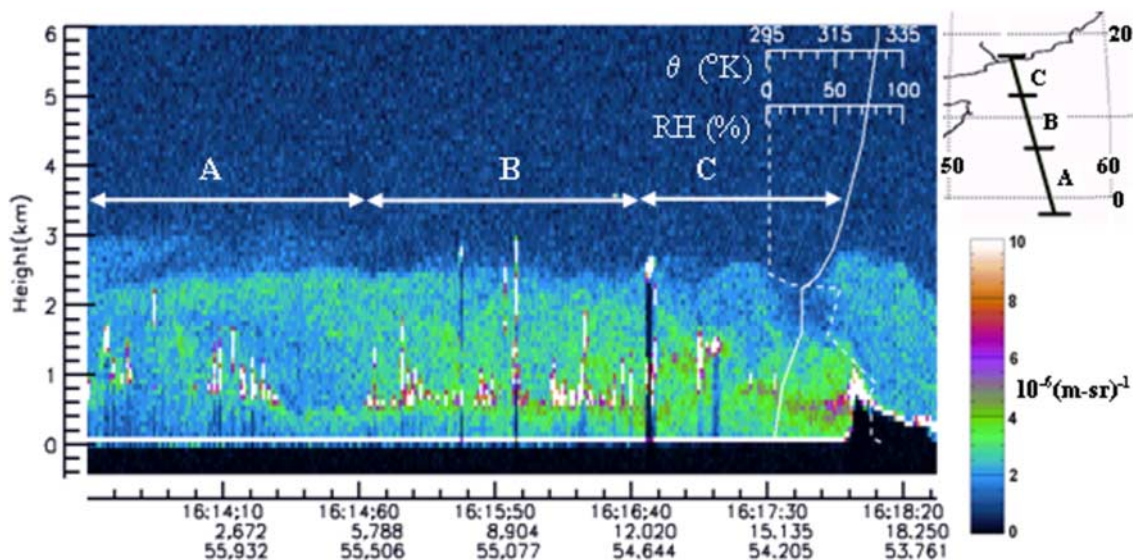


**Figure 2.** Night image of GLAS attenuated backscatter coefficient at 532 nm from western Indian Ocean, October 10, 2003, 16:13:20 to 16:18:30, UTC. The labels of the horizontal axis are UTC time, latitude and longitude. A, B, and C indicate three aerosol regimes that are referred to in the text. The prominent white line at 0 km, rising to 1 km on the right, is the ocean surface and the surface signal from the Saudi Arabian peninsula. The potential temperature (solid line profile) and relative humidity (dash line profile) are shown.

be proportional to the particle number density. Also, a capping temperature inversion exists at about 2.2–2.4 km. In segment B, a relatively strong signal extends from 16:15:00 to about 16:17:10 UTC, about 900 km horizontally. The highest density of clouds also exists in this segment, suggesting a positive relationship between aerosol density and cloud formation. This could result from a mutual correlation to higher relative humidity, a larger concentration of cloud condensation nuclei (CCN), some other effect, or a combination of effects. In the northern end, segment C, the top of the aerosol layer becomes less horizontal and somewhat ragged. A smaller cloud density exists in the north. Visual inspection indicates that cloud bases in segment B are at uniform altitude of about 500 m. The clouds that exist in northern segment C have variable

cloud base heights. Cloud frequency is also lower in the southern segment A, 16:13:20–16:15:00 UTC, where the aerosol density is also lower. In addition, cloud base heights are higher than those in segment B, which suggests a lower layer-average relative humidity in segment A. A separate region of aerosol appears to sit atop the capping inversion at about 16:14:00. A distinct gap occurs between the lower layer and the higher. Backward trajectory computations (not shown) using NOAA Hysplit Model based upon FNL meteorological data indicate that the air above the inversion comes from Africa and the Arabian Peninsula within two to three days of the image. Finally, the cloud elements on either side of 16:15:50 UTC are evidence of local convection breaching the inversion.

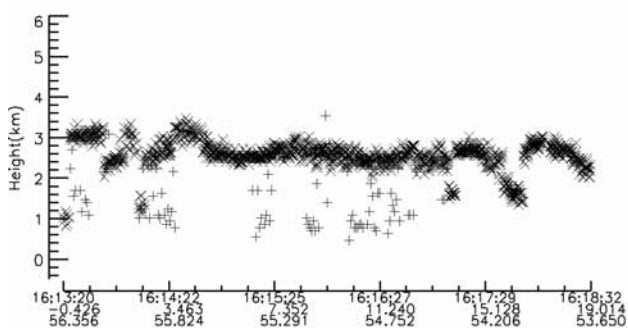


**Figure 3.** Layer tops from GLAS for October 10, 2003. Aerosol layer tops at 5Hz are shown with x and cloud tops at 1Hz are shown with pluses.

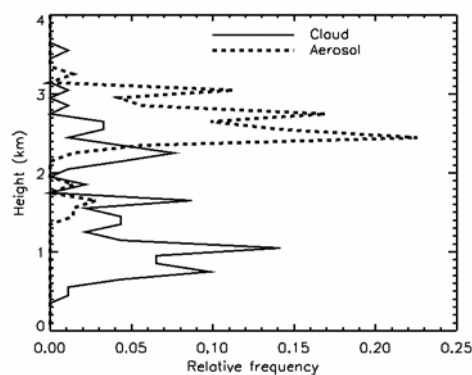


**Figure 4.** GLAS tops of aerosol layer and cloud elements for October 10, 2003, shown as relative frequency of each species. The plots clearly show clouds embedded in the low level aerosol layer.

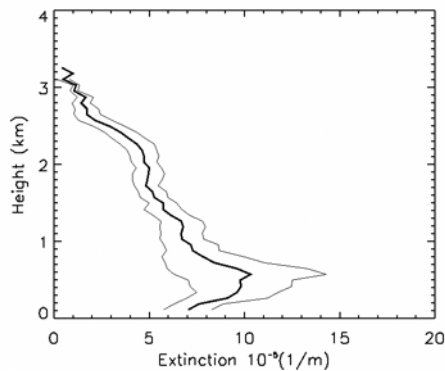


**Figure 5.** Average aerosol extinction coefficient profile from October 10, 2003, 16:13:20–16:17:50 UTC. The light lines show 1 standard deviation range from the mean.

[13] Figure 3 shows objective analysis of layer boundaries based upon GLAS data. The results shown are taken from the routine GLAS product files GLA08 and GLA09 [Spinhirne *et al.*, 2005], hence, they reflect both the successes and failures of production analysis. Aerosol layer boundaries are based on data from the 532 nm channel and cloud boundaries are based on 1064 nm data. The top of the PBL aerosol layer indicated by X's generally agrees with subjective interpretation. PBL top discrepancies include the top of the southern elevated layer and a few cloud elements in the north and south. Cloud tops are shown with plus signs, +. Discrepancies are scattered throughout the image but the cloud tops in segment B are accurately found. Some cloud elements are missed. The errors reinforce the notion of the difficulty of doing such analysis with space borne remote sensing techniques. This analysis is not feasible with passive instruments.

[14] A graphical rendering of the relative positions of cloud embedded in marine aerosol is shown in Figure 4. The graph shows plots of relative frequency of cloud top and aerosol top. The maximums of each of plot give an accurate indication of the vertical location of each species through the data segment. Even with some discrepancies, such as the secondary cloud peak at 2.4 km., it clearly shows clouds embedded in the surface aerosol layer. This type of analysis could be done on a large scale to provide fresh insight and validation of marine boundary layer modeling results.

[15] The extinction coefficient,  $s(z)$ , of aerosol volumes is an important measure of the direct effect of optical scattering and absorption upon the earth's radiation budget and climate [Penner *et al.*, 1998; Sekiguchi *et al.*, 2003]. Extinction coefficient enters into the calculations of incoming and reflected shortwave radiation and outgoing long-wave radiation. The aerosol extinction coefficient profile at 532 nm is a routine GLAS product. The average profile for cloud free columns, computed from data from GLA10 [Spinhirne *et al.*, 2005] for the Indian Ocean segment is shown in Figure 5. In GLAS production,  $s(z)$  [Palm *et al.*, 2002], is computed inside all layers of a vertical column, differentiation between cloud and aerosol, then separated in the final product.. The

profile shows the aerosols extending to maximum height of about 3.1 km. It has a roughly linear increase from 1.8 km down to the maximum at 0.6 km. That is the approximate level of cloud bottoms in segment B. The maximum delineates the level of transition from aerosol to cloud, the lifted condensation level. The magnitude of the average  $s(z)$  decreases rapidly below this level down to the lowest altitude of valid average extinction coefficients, about 0.115 km. With such computations done globally and routinely, statistics of  $s(z)$  will be a major contribution of GLAS to climatological studies of the Earth.

#### 4. Summary and Conclusions

[16] Lidar remote sensing has the advantage of a direct and unambiguous measurement of the height resolved profile of cloud and aerosol scattering layers. Space borne lidar has the advantage of global coverage. The ICESat mission has produced the first such data sets. The GLAS instrument observes all radiatively significant cloud and aerosol to the limit of signal attenuation. As shown in this paper, the data may be used to discriminate between and measure the separate and relative height distribution of aerosol and clouds within typical and polluted boundary layer conditions. The results have applications of inference of direct radiative forcing of aerosol and of the influence between aerosol and clouds. We have found in a case study for the Indian ocean region that clouds may form within and well below thick layers of aerosol loading, as has been reported in aircraft measurements. Studies of this type and others involving clouds, aerosols and their interactions have been demonstrated to be possible with spaceborne lidar on a global basis.

[17] **Acknowledgments.** The authors wish to thank the ICESat SCF data distribution team for making GLAS data available on a timely basis. The Cloud Physics Lidar is sponsored by NASA's Earth Observing System (EOS) office and by NASA Radiation Sciences (Code YS). The ICESat Science Team is also sponsored by the EOS office.

#### References

- Ackerman, A. S., O. B. Toon, D. E. Stevens, A. J. Heymsfield, V. Ramanathan, and E. J. Welton (2000), Reduction of tropical cloudiness by soot, *Science*, *288*, 1042–1047.
- Ackerman, A. S., O. B. Toon, D. E. Stevens, and J. A. Coakley Jr. (2003), Enhancement of cloud cover and suppression of nocturnal drizzle in stratocumulus polluted by haze, *Geophys. Res. Lett.*, *30*(7), 1381, doi:10.1029/2002GL016634.
- Coakley, J. A., Jr., W. R. Tahnk, A. Jayaraman, P. K. Quinn, C. Devaux, and D. Tanré (2002), Aerosol optical depths and direct radiative forcing for INDOEX derived from AVHRR: Theory, *J. Geophys. Res.*, *107*(D19), 8009, doi:10.1029/2000JD000182.
- Palm, S. P. *et al.* (2002), GLAS atmospheric data products, Algorithm Theor. Basis. Doc. ATBD-GLAS-01, version 4.2, Earth Obs. Syst. Proj. Off., Greenbelt, Md. (Available at [http://eospsos.gsfc.nasa.gov/eos\\_homepage/for\\_scientists/atbd/viewInstrument.php?instrument=6.](http://eospsos.gsfc.nasa.gov/eos_homepage/for_scientists/atbd/viewInstrument.php?instrument=6.))
- Penner, J. E., C. C. Chuang, and K. Grant (1998), Climate forcing by carbonaceous and sulfate aerosols, *Clim. Dyn.*, *14*, 839–851.
- Platnick, S., *et al.* (2000), The role of background cloud microphysics in the radiative formation of ship tracks, *J. Atmos. Sci.*, *57*, 2607–2624.
- Rosenfeld, D. (2000), Suppression of rain and snow by urban and industrial air pollution, *Science*, *287*, 1793–1796.
- Sekiguchi, M., T. Nakajima, K. Suzuki, K. Kawamoto, A. Higurashi, D. Rosenfeld, I. Sano, and S. Mukai (2003), A study of the direct and indirect effects of aerosols using global satellite data sets of aerosol and

- cloud parameters, *J. Geophys. Res.*, 108(D22), 4699, doi:10.1029/2002JD003359.
- Spinhirne, J. D., M. Z. Hansen, and L. O. Caudill (1982), Cloud top remote sensing by airborne lidar, *Appl. Opt.*, 21, 1564–1571.
- Spinhirne, J. D., W. D. Hart, and D. L. Hlavka (1996), Cirrus infrared parameters and shortwave reflectance relations from observations, *J. Atmos. Sci.*, 53, 1438–1458.
- Spinhirne, J. D., S. P. Palm, W. D. Hart, D. L. Hlavka, and E. J. Welton (2005), Cloud and aerosol measurements from GLAS: Overview and initial results, *Geophys. Res. Lett.*, 32, L22S05, doi:10.1029/2005GL023507.
- Twomey, S. (1974), Pollution and the planetary albedo, *Atmos. Environ.*, 8, 1251–1256.
- 
- W. D. Hart, D. L. Hlavka, and S. P. Palm, Science Systems and Applications, Inc., NASA GSFC Code 613.1, Greenbelt, MD 20771, USA. (billhart@agnes.gsfc.nasa.gov)
- J. D. Spinhirne, NASA Goddard Space Flight Center, Code 613.1, Greenbelt, MD 20771, USA.